NANO LETTERS

pubs.acs.org/NanoLett Letter

Role of Thin Film Adhesion on Capillary Peeling

Jingcheng Ma,* Jin Myung Kim, Muhammad Jahidul Hoque, Kamila J. Thompson, SungWoo Nam, David G. Cahill, and Nenad Miljkovic*

Cite This: *Nano Lett.* 2021, 21, 9983–9989 Read Online

ACCESS | Metrics & More | Article Recommendations | Supporting Information

ABSTRACT: The capillary force can peel off a substrate-attached film if the adhesion energy (G_w) is low. Capillary peeling has been used as a convenient, rapid, and nondestructive method for fabricating free-standing thin films. However, the critical value of G_w, which leads to the transition between peeling and sticking, remains largely unknown. As a result, capillary peeling remains empirical and applicable to a limited set of materials. Here, we investigate the critical value of G_w and experimentally show the critical adhesion ($G_{w,c}$) to scale with the water−film interfacial energy ($\approx 0.7\gamma_{fw}$), which corresponds well with our theoretical prediction of $G_{w,c} = \gamma_{fw}$. Based on the critical adhesion, we propose quantitative thermodynamic guidelines for designing thin film interfaces that enable successful capillary peeling. The outcomes of this work present a powerful technique for thin film transfer and advanced nanofabrication in flexible photovoltaics, battery materials, biosensing, translational medicine, and stretchable bioelectronics.

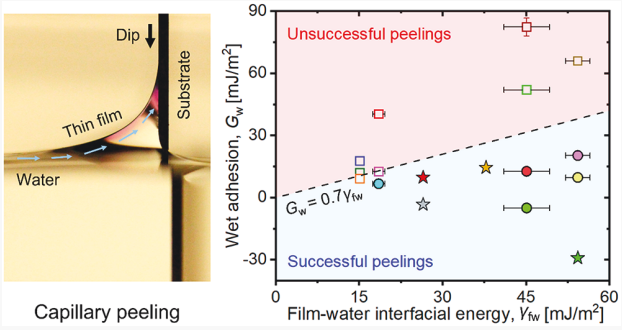

KEYWORDS: *thin film, peeling, capillary, adhesion, surface energy, 2D materials*

Capillary peeling is a phenomenon that occurs when a substrate-attached film detaches by the capillary force when the film−substrate interface contacts water.[1] Capillary peeling has been reported as a rapid and nondestructive method for fabricating free-standing thin films, including polymers,[2−5] biofilms,[6] metallic films,[7,8] or atomically thin two-dimensional (2D) materials.[9,10] The free-standing films not only can be utilized to study material properties such as elasticity,[4,8] rheology[2,3,6] or stress[5] but also can be applied in the fields of electronics[7] and biomedical devices[6] by transferring the films from the host substrate to other surfaces of interest.[11]

Despite many applications of capillary peeling, few have systematically examined the effect of the film−substrate adhesion (G_w), or in general, the surface thermodynamic requirements to ensure peeling success. In this work, we use well-controlled surface chemistries and adhesions to experimentally determine that successful peeling occurs consistently among a variety of substrates and film materials when $G_w < 0.7\gamma_{fw}$, where γ_{fw} is the film−water interfacial energy. This result agrees with our theoretical predictions of $G_w < \gamma_{fw}$. Realizing that the success of capillary peeling relies on other factors such as the film elasticity[1,11,12] and swelling stress,[12] we carefully design experiments where these forces are at least 10^3 times weaker than the surface tension of water, to focus on surface thermodynamics.

To study capillary peeling, we utilized a commonly used sample dipping apparatus[1,11] that slowly dips a vertically oriented thin film-coated surface into a quiescent water bath (Figure 1a). We took images of the sample from the side using a DSLR camera or a high-speed camera (see details of the experimental setup at Supplemental Section S1). To benchmark the peeling process, we used a 59 nm thick Teflon-AF amorphous copolymer (Teflon AF-2400, DuPont) as a model film material that was spun-cast on 1 cm × 2 cm smooth sapphire wafer (c-m plane, University Wafer). Prior to the experiment, we cleave the bottom end of the sample (the one that contacts water) by ∼1 mm using a diamond cutter to prevent excessive polymer warping the edge of the wafer after spin-coating and to ensure that the film−substrate interface is exposed to water during the experiment. If the film is conformal and the boundaries are cleaved, we always obtain a continuous peeled layer.

Our experiment reveals that successful peeling has three stages as shown in Figure 1b. The first stage initiates the contact between the sample and water surface. At this stage, the dipping speed U_I approaches zero, enabling us to exclude the contribution of water viscous dissipation. In our experiments, U_I was controlled manually to ensure that U_I < 0.1 mm/s

Received: September 8, 2021
Revised: November 10, 2021
Published: November 17, 2021

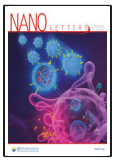

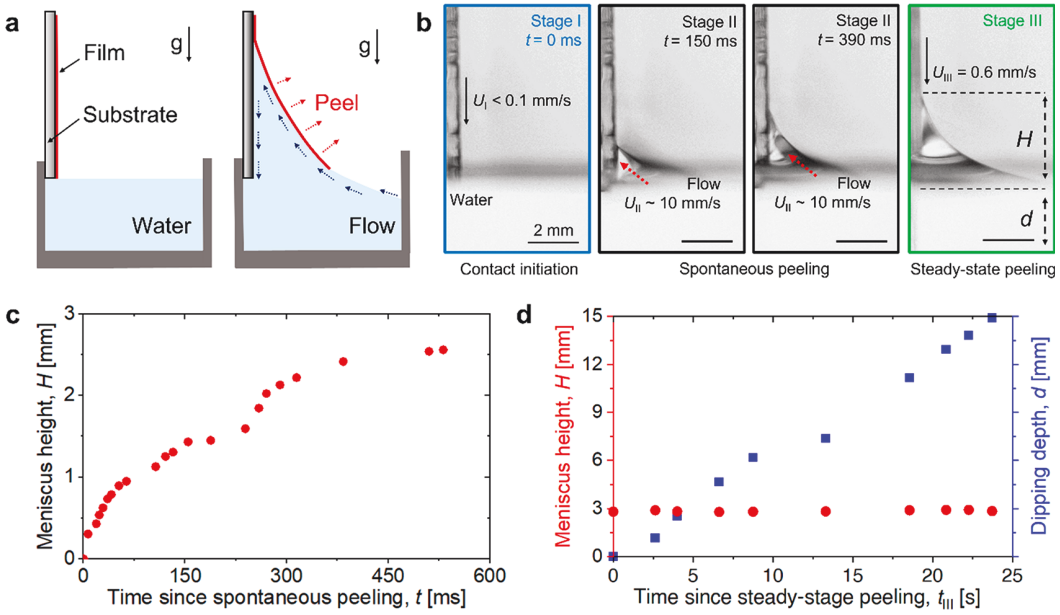

Figure 1. Initiation of capillary peeling. (a) Schematic diagram of the capillary peeling process (diagram not to scale). Water exhibits a split-injection flow pattern as observed by previous work.[1] (b) High-speed time-lapse optical images of the three stages of capillary peeling, including contact initiation (Stage I, $t = 0$), spontaneous initiation of peeling (Stage II, $t = 0$ to 390 ms), and steady-state peeling (Stage III, $t_{III} = 0$ to 24 s). Time $t = 0$ represents the time immediately after contact (±3 ms), and $t_{III} = 0$ represents the time immediately after dipping the sample into water at a constant rate. (c) Time evolution of the meniscus height (H) during peeling initiation (stage II). (d) The time evolution of the meniscus height (H, left red axis) and sample dipping depth (d, right blue axis) during steady-state peeling (stage III). The uncertainty in length measurement was less than 0.1 mm and arises from uncertainty in the pixel location (±3 pixels) within the high-speed imaging experiment. Error bars in (c) and (d) are smaller than the symbol size and are not shown for clarity.

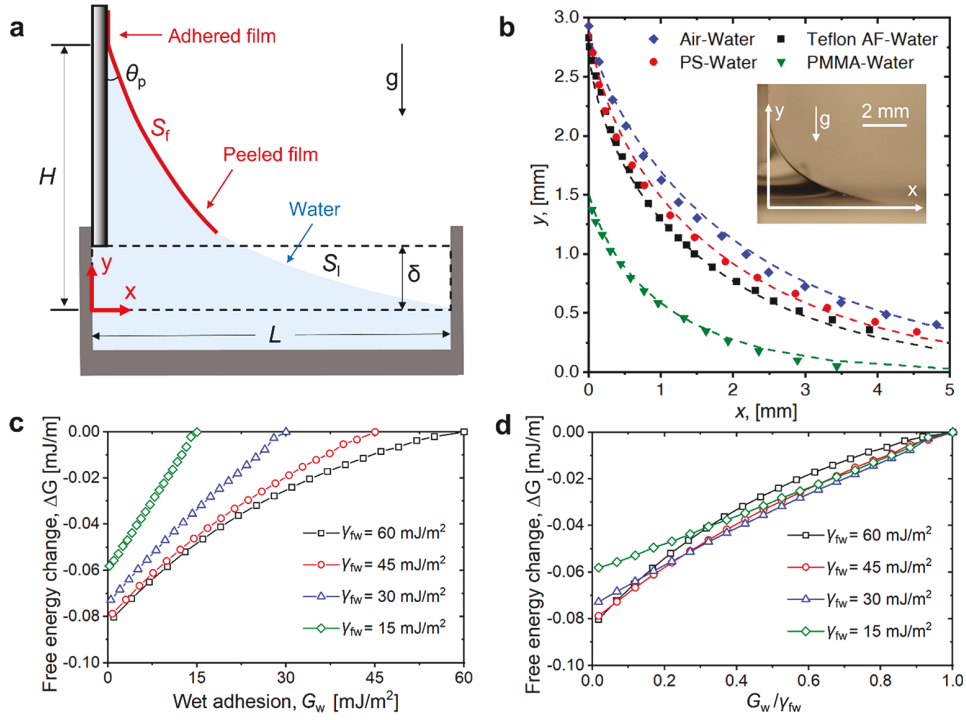

Figure 2. Modeling of the capillary peeling process. (a) Schematic diagram illustrating the two states of water before and after peeling. Schematic not to scale. The black dashed box labels the water plate before capillary peeling. (b) Comparison between experimental (solid dots) and theoretical modeling (dashed lines) of the film meniscus profile. Inset: photograph of the cross-section of the water meniscus. (c) Free energy change per unit film length (ΔG) as a function of wet adhesion (G_w) and film–water interfacial energy (γ_{fw}). (d) Free energy change per unit film length as a function of normalized wet adhesion (G_w/γ_{fw}). The free energy change per unit film length is always negative when $G_w < \gamma_{fw}$. Error bars in (b) are 0.05 mm (±5 pixels) and are smaller than the symbol size, hence are not shown for clarity.

https://doi.org/10.1021/acs.nanolett.1c03494
Nano Lett. 2021, 21, 9983−9989

(measured to be 0.07 ± 0.04 mm/s, see Supplemental Video V1), which results in negligible viscous energy dissipation (see Supplemental Sections S3 and S4). After the interface contacts the water, the second stage spontaneously initiates water flow into the film−substrate interface and forms a dual-section water meniscus. The first section of the water meniscus near the substrate was covered by the peeled free-standing film, while the second section consists of a water meniscus having water−air interface. The time evolution of the peeling height is shown in Figure 1c, demonstrating a characteristic flow speed of $U_{II} \sim 10$ mm/s. The flow during stage II is not continuous as indicated by Figure 1c and Supplemental Video V1. Detailed numerical investigations are needed to fully understand and resolve the complex flow hydrodynamics. Within 0.5 s, the meniscus height reached at an equilibrium position at $H \approx 3$ mm. After the meniscus forms, the sample was manually dipped into the water bath at a speed of $U_{III} \approx 0.6$ mm/s (stage III) and the film was peeled at a constant rate. Although we did not systemically study how U_{III} affects steady peeling, we did observe that once the initial meniscus is formed, steady peeling can be maintained even when U_{III} is as high as 20 mm/s (the speed limitation of our experimental system, see Supplemental Video V2). The depth of the sample and the stabilized meniscus height shown in Figure 1d indicate that the peeling is now in a quasi-equilibrium state. Because U_I in our experiment is negligible when compared to U_{II}, the substrate can be approximated to be stationary during peeling initiation (stage II). This demonstrates that peeling can be spontaneous even when kinetic factors, such as sample dipping velocity, are absent. Therefore, revealing the role of surface thermodynamics is key to understanding the criterion governing successful capillary peeling.

We study the thermodynamic criterion of capillary peeling by analyzing the change in Gibbs free energy, ΔG, between the beginning and the end of stage II, and a negative ΔG indicates that peeling is spontaneous. Note that we mainly consider hydrophobic films here; otherwise, the system free energy can also decrease via formation of a water meniscus on the film. Extra considerations for hydrophilic films are included in Supplemental Section S6. Also note that free energy analysis should be performed in a thermodynamically closed system. As the viscous flow of water during stages I or II bring irreversible energy dissipation, we ignore this dissipation in the initial free energy analysis, later treating it as a correction factor.

We study the energy change in the $x-y$ plane (Figure 2a) and assume the meniscus profile does not vary in the z-axis (2D approximation). Our assumption is deemed appropriate as forces arising from gravity, capillarity, or film stretching do not have z-components. Additional experiments observing the uniformity of both the thin film edge (before peeling) and the peeling front propagation (after peeling) verified this assumption (Supplemental Section S5). In our model, the peeling process is described by a water plate having thickness δ and length L that will be deformed to form a dual-section water meniscus (Figure 2a). The Gibbs free energy change comprises of three reversible energy components: (1) the work of adhesion overcome at the interface between the substrate and the film, (2) the capillary force that stretches the end of the film, and (3) the change in gravitational potential:

$$\Delta G = G_w(H - \delta) + \gamma_l(S_l - L) + \rho g \delta L(y_{c,m} - y_{c,p}) \quad (1)$$

The position $y = 0$ is the water level where $x = L$. Here, H is the equilibrium meniscus height, S_l is the arc length of the water meniscus having a water−air interface, ρ is water's density, g is the gravitational acceleration, $\gamma_l \approx 72$ mN/m is the liquid−vapor surface tension of water at room temperature, and $y_{c,m}$ and $y_{c,p}$ are the centroids of the water before and after peeling, respectively.

Deformation of the film brings extra elastic energy stored in the film, including bending and stretching energy, which relate to thin film thickness, Young's modulus, and Poisson's ratio. However, bending and stretching can be neglected here as most thin polymeric and metallic films (films are thinner than 10 μm) or 2D materials store negligible (<1%) elastic energy when compared to the work done by the capillary force (see Supplemental Section S4 for discussions regarding the threshold of thin film thickness and elasticity). Directly incorporating these terms in our model is beyond the scope of our work, and future work is needed to further understand the threshold film thickness and effect of elasticity to the capillary peeling criterion. Here, our experiments are performed with polymer films that are relatively soft ($E \sim 1$ GPa) and thin ($h \sim 100$ nm). Under these circumstances, the energy-per-meniscus width contributed by the surface tension of water and gravatational potential are both $\sim 10^{-4}$ J/m, with negligible contributions from thin film bending ($\sim 10^{-11}$ J/m) and stretching ($\sim 10^{-7}$ J/m). See Supplemental Section S4 for detailed calculations.

To calculate ΔG, the geometric profile of the dual-section meniscus is required. For the water meniscus having the water−air interface (devoid of the polymer film floating on water, S_l, Figure 2a), the meniscus profile is described by the balance between the gravitational force and Laplace pressure and takes the form of the equation[13]

$$\rho g y = \gamma_l \frac{-\frac{d^2y}{dx^2}}{\left[1 + \left(\frac{dy}{dx}\right)^2\right]^{3/2}} \quad (2)$$

For the thin film meniscus (S_f, Figure 2a), recent work assumed that eq 2 remains valid with the shape of the meniscus not affected by the film.[11] However, we found that the profile of the free water surface meniscus (S_l, Figure 2a) deviates for varying polymeric films, including a 59 nm Teflon-AF film, a 199 nm polystyrene (PS) film, and a 170 nm polymethyl methacrylate (PMMA) film. The thicknesses of the films are measured by ellipsometry. Young's modulus of the Teflon-AF film is measured using the capillary wrinkling technique,[4] which yields $E_{Teflon} = 0.67 \pm 0.04$ GPa (Supplemental Section S7). Young's modulus of commonly used PS and PMMA films are obtained from the literature,[14] both spanning 1−5 GPa. Therefore, the thin film elasticity can be ignored here.

The measured profile of each meniscus is shown in Figure 2b, which indicates that the shape of meniscus can indeed be affected by the change in interfacial tension. Therefore, we replace γ_l in eq 2 with the film−water interfacial tension γ_{fw}. To examine whether modified eq 2 accurately describes the meniscus profile, γ_{fw} must be known. Direct measurements of solid−liquid interfacial tension is challenging due to the presence of material deformation at very small length scales: $\gamma/E \sim 1$ Å.[15] Here, γ_{fw} is approximated using the known solid−liquid interfacial energy, which we measured using the Owens−Wendt method with the apparent contact angle of water and diiodomethane droplets deposited on the film surfaces.[16,17] We emphasize that although the terms "interfacial energy" and "interfacial tension" are usually numerically equivalent for liquid

https://doi.org/10.1021/acs.nanolett.1c03494
Nano Lett. 2021, 21, 9983−9989

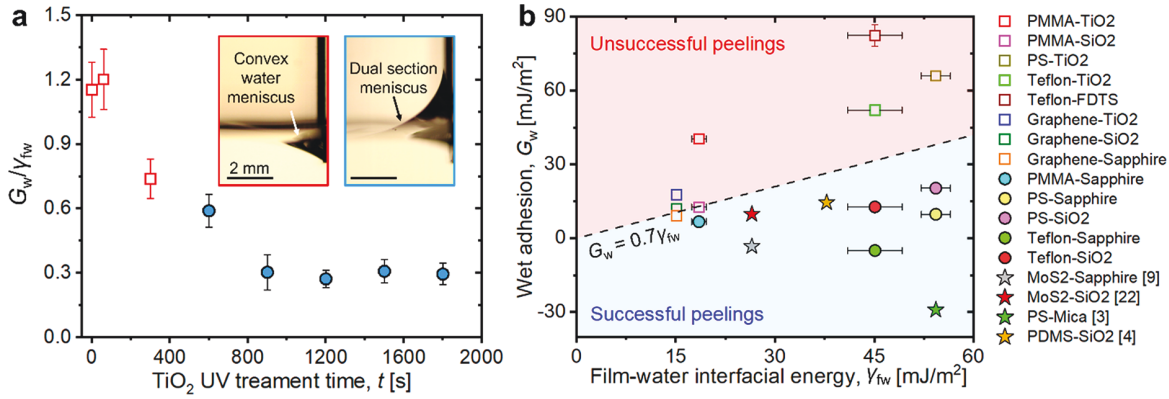

Figure 3. Experimental validation of the peeling criterion ($G_w < \gamma_{fw}$). (a) Ratio of G_w and γ_{fw} of a Teflon-AF/TiO_2 sample as a function of UV exposure time of the TiO_2 prior to Teflon-AF deposition. The results demonstrate that successful peeling occurs when $G_w < 0.7\gamma_{fw}$. (b) Validation of the peeling criterion ($G_w < 0.7\gamma_{fw}$) for a variety of films and substrates. Unsuccessful peeling, successful peeling, and peeling mentioned in literature are shown by hollow squares, solid circles, and solid stars, respectively. The light blue shaded region represents peeling, while the red shaded region represents no peeling.

interfaces and differ for solid interfaces,[18] recent studies have shown that for amorphous polymeric solids, the molecules on the solid surface can have local mobility which allows them to show liquid-like behavior. Thus, the interfacial energy and tension are numerically close for these materials.[19] We further clarify that "interfacial tension" used herein does not represent "interface stress".[20] Interfacial tension describes the new surface formed by the movement of molecules from the bulk of the material to its surface and interface stress describes a surface having constrained surface molecules that has been elastically stretched to increase its surface area. Using the interfacial energies between water and PS (γ_{fw}= 54.3 ± 2.2 mJ/m^2), Teflon-AF (γ_{fw}= 45.1 ± 4.1 mJ/m^2), and PMMA (γ_{fw}= 18.5 ± 1.1 mJ/m^2), we found that modified eq 2 agrees well with our experimental measurements.

It is also important to model the equilibrium angle θ_p formed between the film and substrate at the peeling tip immediately after stage II (Figure 2a), as it represents one of the two boundary conditions required to solve eq 2 ($y' = \cot\theta_p$ at $x = 0$, and $y \to 0$ as $x \to \infty$). Since local stresses from film stretching and bending can be ignored, the force balance at the peeling tip only involves three interfacial energy terms between the film, substrate, and water: $\gamma_{sw} + \gamma_{fw}\cos\theta_p = \gamma_{sf}$, where γ_{sw} and γ_{sf} are the interfacial energies between substrate−water and substrate−film, respectively. Combining this formulation with the definition of wet adhesion, $G_w = \gamma_{sw} + \gamma_{fw} - \gamma_{sf}$, we obtain

$$\cos\theta_p = 1 - \frac{G_w}{\gamma_{fw}} \tag{3}$$

The combination of eqs 1−3 enables us to fully describe the shape of the dual-section water meniscus and to compute ΔG. It is noticeable that both the meniscus shape and free energy are governed only by G_w and γ_{fw}. Therefore, we expect the peeling criterion to take the simple form of $G_w < f(\gamma_w)$ for $\Delta G < 0$. Specifically, eq 3 represents an upper bound of the critical adhesion that yields peeling: $G_w < \gamma_{fw}$. If $G_w > \gamma_{fw}$, the peeling angle $\theta_p > 90°$ makes it physically impossible to open the film−substrate interface. We numerically computed ΔG for a range of G_w and γ_{fw}, with the results summarized in Figure 2c,d. The results indicate that capillary peeling is always a thermodynamically favored process when $G_w < \gamma_{fw}$, showing that γ_{fw} represents not only an upper bound of the critical adhesion but also the exact value of it. Details of the computation of the meniscus profile and ΔG calculations are included in Supplemental Section S2.

To test our framework, we studied the peeling process using a 59 nm thick Teflon-AF film deposited on a smooth TiO_2 surface. A 20 nm thick TiO_2 layer was deposited on a polished Si wafer by atomic layer deposition (Savannah S100 system, Cambridge Nanotech). We used Teflon-AF film as the film materials because of its hydrophobicity and its resistance to swelling, which minimized swelling-induced stress. Furthermore, Teflon-AF has weak polar interaction (polar surface energy component $\gamma_p < 0.5$ mJ/m^2); hence it is not expected to form covalent bonds with TiO_2. In our experimental system, we measure the work of adhesion that only involves van der Waals forces and hydrogen bonds using the Owens−Wendt method.[16,17] The elimination of covalent bonds enables us to approximate the actual wet adhesion from the measured work of adhesion.

The selection of TiO_2 substrate material was rationally done because its surface energy can be tuned with ultraviolet (UV) light exposure.[21] The surface energy of TiO_2 was controlled with the following steps: immediately after (<1 min) deposition of TiO_2 on a polished Si wafer, samples were stored in a sealed polypropylene wafer carrier for at least 4 days prior to conducting peeling experiments. The air trapped inside the wafer carrier contains volatile organic compounds (VOCs) that can adsorb on the TiO_2 surface, lowering its surface energy.[22] The VOC absorption saturated after 4 days as evidenced by the saturation of the advancing contact angle of DI water on the surfaces (70 ± 5° on 5 samples stored for 4 days and another 5 samples stored for 114 days). Next, the TiO_2 surfaces were exposed to UV light (265 nm wavelength, Fisher Scientific UV-Cross-linker FB-UVXL-1000) at a power of 10 mW/cm^2 for 1−30 min to increase their surface energy. Contact angle measurements were performed using DI water and diiodomethane to measure the surface energy, which showed that the surface energy increased from 47 to 75 mJ/m^2 after 15 min of UV treatment. The Teflon-AF film was then spun-coated on the TiO_2 surfaces. The surface energies, interfacial energies, and adhesion measurements are summarized in Supplemental Section S8.

As shown in Figure 3a, peeling occurs on TiO_2 surfaces cleaned by UV exposure for more than 10 min (blue circle data points), where $G_w/\gamma_{fw} < 0.59 \pm 0.08$. Peeling was not observed

https://doi.org/10.1021/acs.nanolett.1c03494
Nano Lett. 2021, 21, 9983−9989

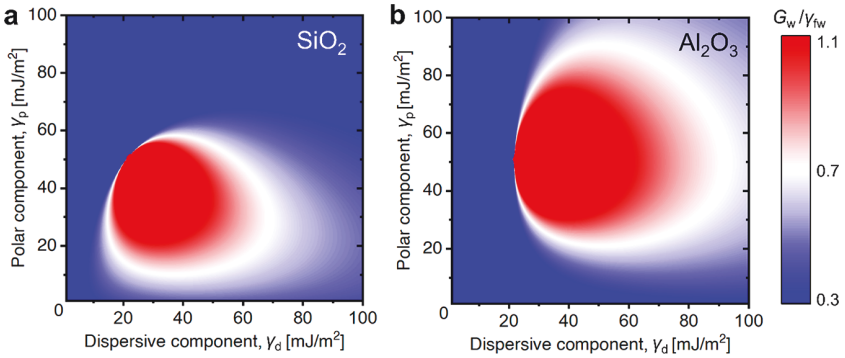

Figure 4. Regime map for successful peeling with respect to film surface energies on smooth thermal SiO_2 and sapphire. Contour map of G_w/γ_{fw} as a function of the film surface energies on (a) polished thermal SiO_2 and (b) polished sapphire wafers. Red regions represent no peeing, while blue regions represent successful peeling.

for $G_w/\gamma_{fw} > 0.74 \pm 0.09$ (red square data points). Hence, the peeling criterion indicated by the experimental results can be approximated by $G_w \approx 0.7\gamma_{fw}$, which corresponds well with our developed model (eq 3).

We hypothesize that the 30% deviation originates from the viscous energy dissipation from the flow of water at stage II. To demonstrate this, the role of sample dipping velocity and viscous dissipation was systematically studied and is included in Supplemental Section S3. We found that the sample dipping velocity at stage I ($U_I < 0.1$ mm/s) is not large enough to create significant viscous flow (viscous force <1% of capillary force). However, the unavoidable spontaneous flow during stage II ($U_{II} \approx 10$ mm/s) creates viscous forces that are roughly 15% of the capillary force, which explains where the deviation in G_w arises from.

To further test our developed criteria, we tested many other thin films, including Teflon-AF, PS, PMMA, and graphene sheets on different substrates including TiO_2, air plasma-cleaned thermal SiO_2/Si, air plasma-cleaned sapphire wafers, and a fluorinated silicon wafer coated with perfluorodecyltrichlorosilane (FDTS). All the surfaces used here were scanned by atomic force microscopy to ensure that the surfaces are smooth enough (roughness ratio <1.01) for contact angle measurement. We found our experimental criterion predicts peeling for most samples (Figure 3b), and the criterion is also appliable to a variety of other test liquids including alcohols and alkanes (see Supplemental Section S9). Other than samples with measured G_w and γ_{fw}, we also found that peeling cases reported in the literature can be predicted with our criterion, including MoS_2 on sapphire[9] and SiO_2,[23] PS on mica,[3] and polydimethylsiloxane (PDMS) on SiO_2,[4] which are also shown in Figure 3b. Our experiments demonstrate that the film adhesion requirement represents a fundamental thermodynamic aspect to the success of capillary peeling.

With our developed understanding of the peeling criterion, we next look to provide design guidelines for the development of films that enables successful capillary peeling on specific substrate materials (Figure 4). Detailed calculation of G_w and γ_{fw} with respect to the surface energies of the coatings and substrates are included in Supplemental Section S8. Substrate materials are characterized by two surface energy components, the dispersive component γ_d that interacts with other materials by van der Waals forces and the polar component γ_p that interacts with other materials by polar forces such as hydrogen bonding.[24] Here, two substrates were considered: thermal SiO_2 on silicon wafer as a commonly used canonical material (Figure 4a) and an air plasma-cleaned sapphire wafer (Figure 4b), which has the highest surface energy (≈100 mJ/m^2) among all surfaces considered here. Figure 4 shows the calculated contour map of G_w/γ_{fw} as a function of film surface energies. Peeling will not occur in the red shaded region where $G_w > 0.7\gamma_{fw}$. There are two distinct cases where peeling can generally occur. The first is when we use a low-surface-energy polymers ($\gamma_d < 30$ mJ/m^2, $\gamma_p < 30$ mJ/m^2), including PMMA, PS, and Teflon, where G_w is relatively low. The second case is with the use of materials that have high film surface energy ($\gamma_d > 50$ mJ/m^2 or $\gamma_p > 50$ mJ/m^2), where γ_{fw} is relatively high. This criterion helps to explain why thin metallic films deposited on SiO_2 can delaminate by water exposure. Previous work attributes peeling to the hydrolysis reaction in water with the covalent Si−O−metal bond.[7,8] Here, we show that van der Waals forces and hydrogen bonding alone may provide a large-enough force for peeling.

In summary, we propose a mechanistic understanding for the design of interfaces for effective capillary peeling from both the aspects of thermodynamics and kinetics. Effective capillary peeling has the potential to advance state-of-the-art nanofabrication techniques. Two main approaches for nanofabrication exist: "top-down"[25] which fabricates layers and patterns them in-place (i.e., nanolithography) and "bottom-up"[26] which assembles basic units into more elaborate structures. Capillary peeling provides the possibility of combing the merits of both established approaches where layer structures fabricated by the top-down approach can be peeled and act as basic units to be deformed or assembled layer-by-layer into functional composites. For example, coupling of semiconductors and metallic films with biofilms and tissues can engineer a variety of bioelectronics interfaces for biosensing,[27−29] tissue engineering,[30] and translational medicine.[31] The rapid, low-cost, scalable, and nondestructive capillary peeling technique studied here has potential for use in a wide range of applications.

■ ASSOCIATED CONTENT

Supporting Information

The Supporting Information is available free of charge at https://pubs.acs.org/doi/10.1021/acs.nanolett.1c03494.

S1. Experimental setup used for the peeling experiment. S2. Free energy change calculations for forming the dual and single section water menisci. S3. The role of sample dipping velocity and viscous dissipation. S4. Estimation of the forces arising from film stretching, bending, and viscous dissipation. S5. Validation of the 2D assumption.

https://doi.org/10.1021/acs.nanolett.1c03494
Nano Lett. 2021, 21, 9983−9989

S6. Extra considerations for hydrophilic films. S7. Thin film and substrate materials fabrication procedures and characterizations. S8. Measurement of surface energy, interfacial energy, wet adhesion, and error analysis. S9. Capillary peeling with different fluids. S10. Captions for Supplemental Videos (PDF)

Video of the sample contacting water with the manual setup (MP4)

Video of sample dipping at 20 mm/s with the motorized setup (MP4)

Video of sample dipping at 0.02 mm/s with the motorized setup (MP4)

AUTHOR INFORMATION

Corresponding Authors

Jingcheng Ma − *Department of Mechanical Science and Engineering, University of Illinois, Urbana, Illinois 61801, United States;* orcid.org/0000-0002-0473-5042; Email: jcma36@illinois.edu

Nenad Miljkovic − *Department of Mechanical Science and Engineering and Department of Electrical and Computer Engineering, University of Illinois, Urbana, Illinois 61801, United States; Materials Research Laboratory, University of Illinois, Urbana, Illinois 61801, United States; International Institute for Carbon Neutral Energy Research (WPI-I2CNER), Kyushu University, Fukuoka 819-0395, Japan;* orcid.org/0000-0002-0866-3680; Email: nmiljkov@illinois.edu

Authors

Jin Myung Kim − *Department of Materials Science and Engineering, University of Illinois, Urbana, Illinois 61801, United States*

Muhammad Jahidul Hoque − *Department of Mechanical Science and Engineering, University of Illinois, Urbana, Illinois 61801, United States;* orcid.org/0000-0002-8036-4511

Kamila J. Thompson − *Department of Electrical and Computer Engineering, The Ohio State University, Columbus, Ohio 43210, United States*

SungWoo Nam − *Department of Mechanical Science and Engineering, Department of Materials Science and Engineering, and Materials Research Laboratory, University of Illinois, Urbana, Illinois 61801, United States;* orcid.org/0000-0002-9719-7203

David G. Cahill − *Department of Mechanical Science and Engineering, Department of Materials Science and Engineering, and Materials Research Laboratory, University of Illinois, Urbana, Illinois 61801, United States*

Complete contact information is available at: https://pubs.acs.org/10.1021/acs.nanolett.1c03494

Notes

The authors declare no competing financial interest.

ACKNOWLEDGMENTS

The authors gratefully acknowledge funding support from the Office of Naval Research (ONR) under grant No. N00014-16-1-2625. The authors also gratefully acknowledge funding support from the International Institute for Carbon Neutral Energy Research (WPI-I2CNER), sponsored by the Japanese Ministry of Education, Culture, Sports, Science and Technology. J.M. gratefully acknowledges funding support from the PPG-MRL assistantship. This research was partially supported by the NSF through the University of Illinois at Urbana−Champaign Materials Research Science and Engineering Center DMR-1720633.

REFERENCES

(1) Khodaparast, S.; Boulogne, F.; Poulard, C.; Stone, H.A. Water-Based Peeling of Thin Hydrophobic Films. *Phys. Rev. Lett.* **2017**, *119* (15), 154502.

(2) Si, L.; Massa, M.V.; Dalnoki-Veress, K.; Brown, H.R.; Jones, R. A. L. Chain entanglement in thin freestanding polymer films. *Phys. Rev. Lett.* **2005**, *94* (12), 127801.

(3) Pye, J. E.; Roth, C.B. Two Simultaneous Mechanisms Causing Glass Transition Temperature Reductions in High Molecular Weight Freestanding Polymer Films as Measured by Transmission Ellipsometry. *Phys. Rev. Lett.* **2011**, *107* (23), 235701.

(4) Huang, J.; Juszkiewicz, M.; de Jeu, W. H.; Cerda, E.; Emrick, T.; Menon, N.; Russell, T. P. Capillary wrinkling of floating thin polymer films. *Science* **2007**, *317* (5838), 650−653.

(5) Stafford, C. M.; Harrison, C.; Beers, K. L.; Karim, A.; Amis, E. J.; Vanlandingham, M. R.; Kim, H. C.; Volksen, W.; Miller, R. D.; Simonyi, E. E. A buckling-based metrology for measuring the elastic moduli of polymeric thin films. *Nat. Mater.* **2004**, *3* (8), 545−550.

(6) Yan, J.; Moreau, A.; Khodaparast, S.; Perazzo, A.; Feng, J.; Fei, C.; Mao, S.; Mukherjee, S.; Kosmrlj, A.; Wingreen, N.S.; Bassler, B.L.; Stone, H.A. Bacterial Biofilm Material Properties Enable Removal and Transfer by Capillary Peeling. *Adv. Mater.* **2018**, *30* (46), 1804153.

(7) Lee, C. H.; Kim, J. H.; Zou, C. Y.; Cho, I. S.; Weisse, J. M.; Nemeth, W.; Wang, Q.; Van Duin, A. C. T.; Kim, T. S.; Zheng, X. L. Peel-and-Stick: Mechanism Study for Efficient Fabrication of Flexible/Transparent Thin-film Electronics. *Sci. Rep.* **2013**, *3* (2917), 2917.

(8) Kim, J. H.; Nizami, A.; Hwangbo, Y.; Jang, B.; Lee, H. J.; Woo, C. S.; Hyun, S.; Kim, T. S. Tensile testing of ultra-thin films on water surface. *Nat. Commun.* **2013**, *4* (2520), 2520.

(9) Gurarslan, A.; Yu, Y. F.; Su, L. Q.; Yu, Y. L.; Suarez, F.; Yao, S.; Zhu, Y.; Ozturk, M.; Zhang, Y.; Cao, L. Y. Surface-Energy-Assisted Perfect Transfer of Centimeter-Scale Mono layer and Few-Layer MoS2 Films onto Arbitrary Substrates. *ACS Nano* **2014**, *8* (11), 11522−11528.

(10) Woo, G.; Kim, H.U.; Yoo, H.; Kim, T. Recyclable free-polymer transfer of nano-grain MoS2 film onto arbitrary substrates. *Nanotechnology* **2021**, *32* (4), 045702.

(11) Zhang, Y.; Yin, M. T.; Baek, Y.; Lee, K.; Zangari, G.; Cai, L. H.; Xu, B. X. Capillary transfer of soft films. *Proc. Natl. Acad. Sci. U. S. A.* **2020**, *117* (10), 5210−5216.

(12) Baxamusa, S. H.; Stadermann, M.; Aracne-Ruddle, C.; Nelson, A. J.; Chea, M.; Li, S. L.; Youngblood, K.; Suratwala, T. I. Enhanced Delamination of Ultrathin Free-Standing Polymer Films via Self-Limiting Surface Modification. *Langmuir* **2014**, *30* (18), 5126−5132.

(13) De Gennes, P.-G.; Brochard-Wyart, F.; Quéré, D. *Capillarity and wetting phenomena: drops, bubbles, pearls, waves*; Springer Science & Business Media, New York, NY; 2013, pp 43−47.

(14) Xie, X.; Yang, K.X.; Li, D.Y.; Tsai, T.H.; Shin, J.; Braun, P.V.; Cahill, D.G. High and low thermal conductivity of amorphous macromolecules. *Phys. Rev. B: Condens. Matter Mater. Phys.* **2017**, *95* (3), 035406.

(15) Marchand, A.; Das, S.; Snoeijer, J.H.; Andreotti, B. Contact Angles on a Soft Solid: From Young's Law to Neumann's Law. *Phys. Rev. Lett.* **2012**, *109* (23), 236101.

(16) Owens, D. K. Some Thermodynamic Aspects of Polymer Adhesion. *J. Appl. Polym. Sci.* **1970**, *14* (7), 1725.

(17) Ma, J.; Cahill, D. G.; Miljkovic, N. Condensation Induced Blistering as a Measurement Technique for the Adhesion Energy of Nanoscale Polymer Films. *Nano Lett.* **2020**, *20* (5), 3918−3924.

(18) Orowan, E. Surface Energy and Surface Tension in Solids and Liquids. *Proc. R. Soc. Lond. A* **1970**, *316* (1527), 473−491.

(19) Mondal, S.; Phukan, M.; Ghatak, A. Estimation of solid−liquid interfacial tension using curved surface of a soft solid. *Proc. Natl. Acad. Sci. U. S. A.* **2015**, *112* (41), 12563.
(20) Zhang, X. J.; Cahill, D. G. Measurements of interface stress of silicon dioxide in contact with water-phenol mixtures by bending of microcantilevers. *Langmuir* **2006**, *22* (21), 9062−9066.
(21) Wang, R.; Hashimoto, K.; Fujishima, A.; Chikuni, M.; Kojima, E.; Kitamura, A.; Shimohigoshi, M.; Watanabe, T. Light-induced amphiphilic surfaces. *Nature* **1997**, *388* (6641), 431−432.
(22) Yan, X.; Huang, Z. Y.; Sett, S.; Oh, J.; Cha, H.; Li, L. N.; Feng, L. Z.; Wu, Y. F.; Zhao, C. Y.; Orejon, D.; Chen, F.; Miljkovic, N. Atmosphere-Mediated Superhydrophobicity of Rationally Designed Micro/Nanostructured Surfaces. *ACS Nano* **2019**, *13* (4), 4160−4173.
(23) Gaur, A. P. S.; Sahoo, S.; Ahmadi, M.; Dash, S. P.; Guinel, M. J. F.; Katiyar, R. S. Surface Energy Engineering for Tunable Wettability through Controlled Synthesis of MoS2. *Nano Lett.* **2014**, *14* (8), 4314−4321.
(24) Fowkes, F. M. Additivity of Intermolecular Forces at Interfaces 0.1. Determination of Contribution to Surface and Interfacial Tensions of Dispersion Forces in Various Liquids. *J. Phys. Chem.* **1963**, *67* (12), 2538−2541.
(25) Yu, H. D.; Regulacio, M. D.; Ye, E.; Han, M. Y. Chemical routes to top-down nanofabrication. *Chem. Soc. Rev.* **2013**, *42* (14), 6006−6018.
(26) Ariga, K.; Hill, J. P.; Ji, Q. M. Layer-by-layer assembly as a versatile bottom-up nanofabrication technique for exploratory research and realistic application. *Phys. Chem. Chem. Phys.* **2007**, *9* (19), 2319−2340.
(27) Fang, Y.; Prominski, A.; Rotenberg, M. Y.; Meng, L. Y.; Ledesma, H. A.; Lv, Y. Y.; Yue, J. P.; Schaumann, E.; Jeong, J.; Yamamoto, N.; Jiang, Y. W.; Elbaz, B.; Wei, W.; Tian, B. Z. Micelle-enabled self-assembly of porous and monolithic carbon membranes for bioelectronic interfaces. *Nat. Nanotechnol.* **2021**, *16* (2), 206−213.
(28) Kim, D. H.; Lu, N. S.; Ma, R.; Kim, Y. S.; Kim, R. H.; Wang, S. D.; Wu, J.; Won, S. M.; Tao, H.; Islam, A.; Yu, K. J.; Kim, T. I.; Chowdhury, R.; Ying, M.; Xu, L. Z.; Li, M.; Chung, H. J.; Keum, H.; McCormick, M.; Liu, P.; Zhang, Y. W.; Omenetto, F. G.; Huang, Y. G.; Coleman, T.; Rogers, J. A. Epidermal Electronics. *Science* **2011**, *333* (6044), 838−843.
(29) Wang, S. H.; Xu, J.; Wang, W. C.; Wang, G. J. N.; Rastak, R.; Molina-Lopez, F.; Chung, J. W.; Niu, S. M.; Feig, V. R.; Lopez, J.; Lei, T.; Kwon, S. K.; Kim, Y.; Foudeh, A. M.; Ehrlich, A.; Gasperini, A.; Yun, Y.; Murmann, B.; Tok, J. B. H.; Bao, Z. A. Skin electronics from scalable fabrication of an intrinsically stretchable transistor array. *Nature* **2018**, *555* (7694), 83−88.
(30) Tian, B. Z.; Lieber, C. M. Synthetic Nanoelectronic Probes for Biological Cells and Tissues. *Annu. Rev. Anal. Chem.* **2013**, *6*, 31−51.
(31) Koh, A.; Kang, D.; Xue, Y.; Lee, S.; Pielak, R.M.; Kim, J.; Hwang, T.; Min, S.; Banks, A.; Bastien, P.; Manco, M.C.; Wang, L.; Ammann, K.R.; Jang, K.I.; Won, P.; Han, S.; Ghaffari, R.; Paik, U.; Slepian, M.J.; Balooch, G.; Huang, Y.G.; Rogers, J.A. A soft, wearable microfluidic device for the capture, storage, and colorimetric sensing of sweat. *Sci. Transl. Med.* **2016**, *8* (366), 366ra165.

https://doi.org/10.1021/acs.nanolett.1c03494
Nano Lett. 2021, 21, 9983−9989